IEEE Access
Multidisciplinary ⋮ Rapid Review ⋮ Open Access Journal

Received 25 October 2023, accepted 17 December 2023, date of publication 8 January 2024, date of current version 11 March 2024.

Digital Object Identifier 10.1109/ACCESS.2024.3350631

APPLIED RESEARCH

Flexible Calibration Method and Application of Passenger Car HUD Detection Based on Collaborative Robot

DING ZHIGANG[1,2], YANLU LV[1,2], LINGHUA KONG[1,2], ZHIMING DONG[3], JISHI ZHENG[3], JIADI ZHANG[4], AND JIAXIN LIU[2]

[1]School of Mechanical and Automotive Engineering, Fujian University of Technology, Fuzhou 350118, China
[2]Digital Fujian Industry Manufacturing Internet of Things Laboratory, Fujian University of Technology, Fuzhou 350118, China
[3]School of Transportation, Fujian University of Technology, Fuzhou 350118, China
[4]Xiamen Richen Technology Company Ltd., Xiamen 361000, China

Corresponding author: Linghua Kong (15392030898@163.com)

This work was supported by Xiamen Richen Technology Company Ltd., Fujian.

ABSTRACT At present, the HUD calibration of the whole vehicle enterprise adopts the traditional physical Master Gauge to calibrate the camera, and the scheme has low flexibility, occupies a large space, and is unsuitable for the mixed production of different types of vehicles. A flexible calibration approach is presented based on collaborative robots for HUD inspection of passenger cars. They are considering that the general HUD (Head-Up Display) virtual image distance is 2-3 m. A 2.3 m hand-eye calibration method is investigated by mounting a monocular camera on a collaborative robot, considering the effect of ambient light on long-distance hand-eye calibration, and employing customized alumina calibration plates and lighting through appropriate angles. Using the area_scan_polynomial model for camera calibration, the camera's internal reference is solved, and the average error of the resulting camera's internal reference is about 0.15. Compared with the master gauge camera calibration, it shows higher flexibility. The hand-eye calibration results show that the Translation part's maximum error is about 1mm, the maximum error of the Rotational position is about 0.1 degree, and the camera calibration error is within 0.08 pixels. For repeatability, the median of Translation RMS was 0.5 with an interquartile range of 0.171, and the median of Translation Maximum was 0.972 with an interquartile range of 0.216. The median of Rotation RMS was 0.0325 with an interquartile range of 0.0125. The median of the Rotation Maximum was 0.059, with an interquartile range of 0.016. The data of translation is relatively scattered, with an extensive range of changes, but it still maintains a certain repeatability. The Rotation data is relatively stable, with a small degree of change and good repeatability, further meeting the use requirements in the final inspection HUD scene of the whole vehicle.

INDEX TERMS Eye-in-hand, hand-eye calibration, HUD, camera calibration, cooperative robot, repeatability.

I. INTRODUCTION

In recent years, HUDs have gained widespread attention and popularity due to their excellent performance on driver safety features in self-driving cars [1]. When the HUD system is activated, light is emitted from the source through two free-form mirrors and reflected onto the windshield, where it enters the human eye after being reflected through the windshield, forming a virtual image suspended behind the windscreen. Reference [2] The distance between the virtual image and the human eye is known as the virtual image distance, which is a crucial parameter for evaluating the performance of a HUD system. Generally, the virtual image distance of HUD is around 1.8-2.5m. The new generation of Augmented Reality Heads-Up Display (AR-HUD) has a virtual image distance of 7m or more. The projection is

The associate editor coordinating the review of this manuscript and approving it for publication was Tai-Hoon Kim.

located near the front part of the vehicle's hood above the [3]. The standard detection methods for HUDs are manual detection methods and imaging optical system detection methods [4]. Manual testing is mainly done through the inspector observing the HUD projection image and subjective judgment of the HUD display image. The disadvantage is that it can not quantify the data and can not achieve repeatable and accurate measurements. Xiaofeng et al. [5] A study on the luminance perception characteristics of nighttime head-up display (HUD) information was conducted. A brightness-adjustable HUD system was used in this experiment, and the brightness adjustment curve and driver brightness perception model were established with 100 drivers. The study summarizes the brightness pattern of using an in-vehicle HUD under night vision conditions. The imaging optical system inspection method is mainly used to localize and measure the image projected by the HUD using imaging devices such as machine vision, which excels in fast imaging, ranging, and localization. Jun and Miao [6] To improve the accuracy and efficiency of parallax adjustment for flat panel displays, Liu Jun et al. designed a specialized optical system for CCD cameras to achieve HUD parallax measurement. This design constructed a complex and compact approach to combine high-quality image quality with image processing technology, thus making the measurement results more objective and reliable.

At present, the HUD calibration of the vehicle enterprise adopts the traditional Master Gauge to calibrate the camera to carry out HUD detection; the program has some limitations, such as the need to frequently replace and adjust the Master Gauge in different scenes and applications, the degree of flexibility of the Master Gauge is low and occupies a large amount of space, which is not suitable for the production of different types of vehicles in the mixed line production, which leads to a reduction in the efficiency of the display, and at the same time, the program does not have the hand-eye calibration will lead to the accumulation of errors, the HUD system is unstable, and so on a series of problems. The camera is calibrated through a hole in the Master Gauge, as shown in Figure 1. To solve this problem, machine vision technology was used to achieve accurate camera calibration without relying on the Master Gauge's complex structure and to perform precise hand-eye calibration simultaneously.

This calibration method based on machine vision technology solves traditional Master Gauge limitations and provides higher accuracy and stability of HUD inspection results. Accurate hand-eye calibration is critical to achieving precise camera positioning and attitude estimation, eliminating the effects of error accumulation and ensuring system stability and reliability. Therefore, the accuracy of the hand-eye calibration is essential for accurately accomplishing the HUD detection task. 1989 by Tsai and Lenz [7] The first published study of hand-eye calibration divides the problems into two broad categories by placing the calibration matrices in the order in which they are solved. First, the first category is

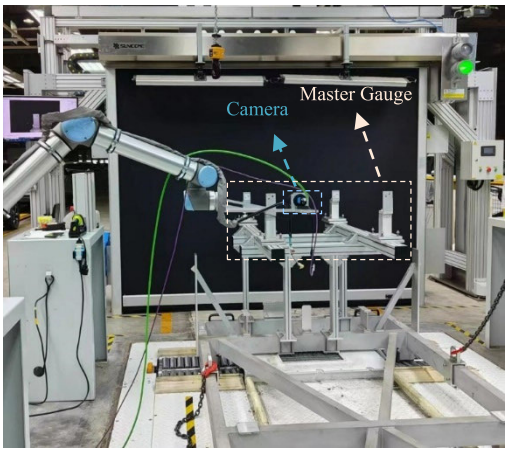

FIGURE 1. Master Gauge.

by solving the rotation matrix first and then the translation vectors: Classical algorithms such as Chou and Kamel [8] A closed-loop linear solution in hand-eye calibration using quaternions is proposed; Daniilidis [9] The use of pairwise quaternions for hand-eye calibration is proposed; Malti and Barreto [10] For the hand-eye calibration problem in endoscopic cameras used for surgery and 3D visualization, a method for solving the hand-eye calibration matrix using dyadic quaternions is proposed. The second category is by solving the rotation matrix and translation vector simultaneously: E.g. Andreff et al. [11] A closed-loop solution for hand-eye calibration based on matrix direct product is proposed; Li et al. [12] Introducing Kronecker products and pairwise quaternions to solve rotation and translation problems in hand-eye calibration simultaneously; Zhao [13] A new convex optimization L_∞- paradigm optimization is proposed to solve the problem of hand-eye calibration. There are fewer studies on HUD inspection using hand-eye calibration after HUD inspection; to make HUD inspection more flexible while improving productivity, this paper investigates hand-eye calibration in HUD application scenarios.

For traditional enterprises, only through the Master Gauge for camera calibration and thus the limitations of HUD detection, while no hand-eye calibration will lead to the accumulation of errors, the HUD system is not stable and a series of problems, taking into account the general HUD system virtual image projection in the 1.8-2.5 meters or so. A hand-eye calibration method based on a monocular camera is proposed, carried out at 2.3 m from the camera to the calibration plate. The calibration is carried out by first considering the influence of the light source on the calibration by using a customized calibration plate and stripping the light source to strike the light from a suitable angle. Secondly, the camera is calibrated to obtain the internal reference of the camera, while the hand-eye calibration images are used to remove the distortion introduced by the camera lens. Finally, the transformation matrix between the camera and the robot

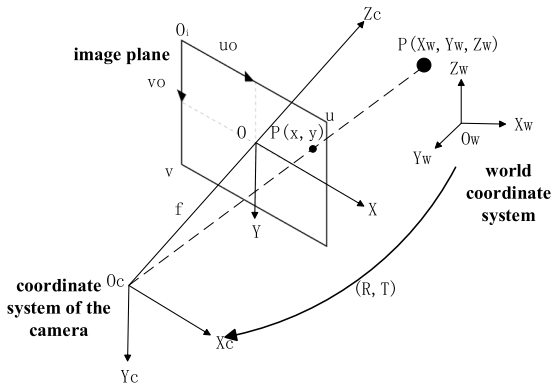

FIGURE 2. Pinhole imaging model.

hand is calculated by performing hand-eye calibration of the camera and the robot for subsequent use in HUD detection.

II. SYSTEM CALIBRATION

A. CAMERA CALIBRATION

The hand-eye calibration process involves the robot capturing images of its surroundings using a camera and using these images to calculate the robot's position and orientation in 3D space to achieve the effect of sensing the environment. The pinhole imaging model is used to describe how the camera projects real-world objects onto the camera's imaging plane, that is, the conversion relationship between the position of a point in real space and its projected work on the camera's ideal imaging plane [14] as shown in Figure 2.

The relationship between the 3D geometric position of a feature point P(Xw, Yw, Zw) on the surface of an object in space and its corresponding point p(x,y) in the image can be obtained by performing coordinate transformations between four coordinate systems. These four coordinate systems include the camera coordinate system (Oc, Xc, YC, Zc), pixel coordinate system (Oi,u,v), image coordinate system (O, X, Y), and world coordinate system (Ow, Xw, Yw, Zw). Where the transformation relationship between the coordinates (Xw, Yw, Zw) of the feature point P in the world coordinate system and the coordinates (Xc, Yc, Zc) in the camera coordinate system can be represented as [15]

$$\begin{bmatrix} X_c \\ Y_c \\ Z_c \\ 1 \end{bmatrix} = \begin{bmatrix} \mathbf{R}_{3\times3} & \mathbf{T}_{3\times1} \\ \mathbf{0}_{1\times3} & \mathbf{1}_{1\times1} \end{bmatrix} \begin{bmatrix} X_w \\ Y_w \\ Z_w \\ 1 \end{bmatrix} = \begin{bmatrix} r_{11} & r_{12} & r_{13} & t_x \\ r_{21} & r_{22} & r_{23} & t_y \\ r_{31} & r_{32} & r_{33} & t_z \\ 0 & 0 & 0 & 1 \end{bmatrix} \begin{bmatrix} X_w \\ Y_w \\ Z_w \\ 1 \end{bmatrix} \tag{1}$$

where R is the rotation matrix (Oc, Xc, YC, Zc) from the world coordinate system (Ow, Xw, Yw, Zw) to the camera coordinate system is an element of R. R can be expressed explicitly as in (2), shown at the bottom of the next page.

From Eq. R is an orthogonal matrix with three degrees of freedom, ψ, θ, ϕ re the three rotation angles of R;t_x, t_y, t_z are the elements of the translation vector T from the world coordinate system to the camera coordinate system. The external parameters of the camera are formed by the rotation matrix R(ψ, θ, ϕ) and, the translation vector T. (t_x, t_y, t_z)

The geometric transformation of projecting an object point onto a 2D image plane in 3D space can be described using a perspective projection model. Using the principle of similar triangles, the transformation relationship between the object point P(Xc, Yc, Zc) in the camera coordinate system and the image point p(x,y) in the image coordinate system can be derived, namely:

$$\begin{cases} \frac{x}{X_c} = \frac{f}{Z_c} \\ \frac{y}{Y_c} = \frac{f}{Z_c} \end{cases} \Rightarrow Z_c \begin{bmatrix} x \\ y \\ 1 \end{bmatrix} = \begin{bmatrix} f & 0 & 0 & 0 \\ 0 & f & 0 & 0 \\ 0 & 0 & 1 & 0 \end{bmatrix} \begin{bmatrix} X_c \\ Y_c \\ Z_c \\ 1 \end{bmatrix} \tag{3}$$

Eq. f is the focal length, and (x, y) denotes the information about the corresponding position of a point in space in the image plane coordinate system.

Assuming that the origin O of the image coordinate system is located at (uo,vo) in the pixel coordinate system and assuming that the image sensor's pixel array is rectangular while ignoring non-rectangular influences, the following relationship exists between the image coordinates (x, y) and the pixel coordinates (u, v).

$$\begin{bmatrix} u \\ v \\ 1 \end{bmatrix} = \begin{bmatrix} \frac{1}{dx} & 0 & u_0 \\ 0 & \frac{1}{dy} & v_0 \\ 0 & 0 & 1 \end{bmatrix} \begin{bmatrix} x \\ y \\ 1 \end{bmatrix} \tag{4}$$

In Eq. is the corresponding physical size of a single pixel point in the x-axis and y-axis directions in mm. (u, v) denotes the corresponding position of a point in space under the pixel coordinate system of the image, and (uo,vo) represents the corresponding pixel coordinate of the origin of the plane coordinate system under the pixel coordinate system.

Summarizing (1) to (4), we obtain the transformation relationship between the world coordinate system and the image pixel coordinate system with the expression:

$$\begin{bmatrix} u \\ v \\ 1 \end{bmatrix} = \frac{1}{z_C} \begin{bmatrix} \frac{f}{d_x} & 0 & u_0 & 0 \\ 0 & \frac{f}{d_y} & v_0 & 0 \\ 0 & 0 & 1 & 0 \end{bmatrix} \begin{bmatrix} R_{3\times3} & T_{3\times1} \\ 0 & 1 \end{bmatrix} \begin{bmatrix} X_W \\ Y_W \\ Z_W \\ 1 \end{bmatrix} \tag{5}$$

define the focal length of the camera as (f_x, f_y):

$$\begin{aligned} f_x &= \frac{f}{d_x} \\ f_y &= \frac{f}{d_y} \end{aligned} \tag{6}$$

Collating (5) and (6) yields:

$$\begin{bmatrix} u \\ v \\ 1 \end{bmatrix} = \frac{1}{z_C} \begin{bmatrix} f_x & 0 & u_0 & 0 \\ 0 & f_y & v_0 & 0 \\ 0 & 0 & 1 & 0 \end{bmatrix} \begin{bmatrix} R_{3\times3} & T_{3\times1} \\ 0 & 1 \end{bmatrix} \begin{bmatrix} X_W \\ Y_W \\ Z_W \\ 1 \end{bmatrix} \tag{7}$$

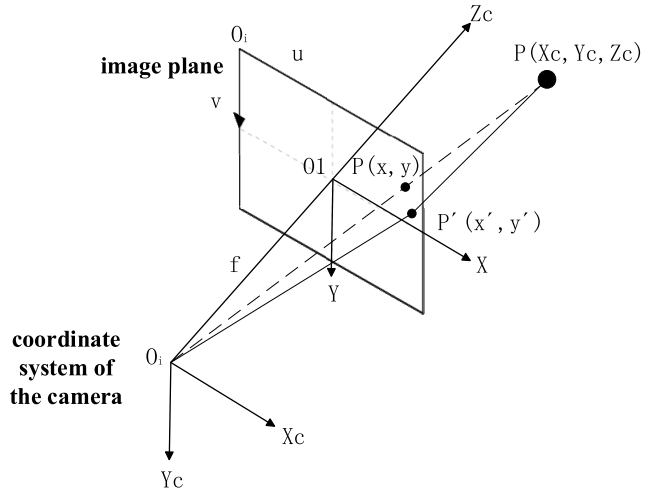

FIGURE 3. Image point position shift due to lens aberration.

B. CAMERA LENS DISTORTION

The process of camera calibration is to find the internal and external parameter matrices of the camera; however, in the actual application scenario, the camera lens in the imaging process due to the lens processing technology and the camera's manufacturing technology level of the camera's projection relationship can not be described by a pinhole model. Instead of following the ideal pinhole imaging pattern exactly, natural optical systems are subject to lens aberrations that cause the pixel position of an object in three-dimensional space on a two-dimensional imaging plane to deviate from the ideal place. This optical error is significantly pronounced when spatial object points form the actual image on the camera's imaging plane, especially in the edge regions of the lens. When using a wide-angle lens, the portion of the image plane away from the center tends to be significantly distorted [16]. Aberration will lead to the optical system imaging position, shape, size, and other aspects of the deviation, thus affecting the imaging quality. For example, in Figure 3, aberration is caused by the change in the image point position in the image plane. Theoretically, the image point coordinates for the P (X, Y). Still, due to the camera aberration, the actual image point becomes P ′(X, ′Y ′), so it is necessary to correct for the monster.

In-camera lens aberrations are mainly categorized into radial and tangential freaks. Face array cameras in Halcon can be used to solve for abnormalities using are_scan_division and area_scan_polynomial models. The camera distortion model in are_scan_division mode considers only radial distortion, a linear distortion model that can be solved inversely to obtain the model parameters. This can be expressed in equation (8):

$$\begin{bmatrix} u'' \\ v'' \end{bmatrix} = \frac{2}{1+\sqrt{1-\left(u^2+v^2\right)}} \begin{bmatrix} u \\ v \end{bmatrix} \tag{8}$$

However, the area_scan_polynomial camera distortion model is a nonlinear distortion model that considers both radial and tangential distortion. The model uses three parameters, K1, K2, and K3, for radial distortion and two parameters, P1 and P2, for tangential distortion. Since the model is nonlinear, the distortion parameter solution is irreversible [17]. The mathematical expression for the camera distortion model for conversion from a distorted image plane coordinate system to a non-distorted image plane coordinate system is:

$$\begin{aligned} u &= \tilde{u} + \tilde{u}\left(K_1 r^2 + K_2 r^4 + K_3 r^6\right) \\ &\quad + 2P_1\tilde{u}\tilde{v} + P_2\left(r^2 + 2\tilde{u}^2\right) \\ v &= \tilde{v} + \tilde{v}\left(K_1 r^2 + K_2 r^4 + K_3 r^6\right) \\ &\quad + P_1\left(r^2 + 2\tilde{v}^2\right) + 2P_2\tilde{u}\tilde{v} \end{aligned} \tag{9}$$

where $r = \sqrt{\tilde{v}^2 + \tilde{u}^2}$, To obtain higher calibration accuracy, this paper uses area_scan_polynomia for aberration solving [18].

C. CAMERA PARAMETER ACQUISITION

Halcon is a machine vision software developed by the German company MVtec, which has a rich set of built-in function operators and examples covering a wide range of functions such as filtering, morphological processing, classification, etc., enabling users to develop industrial vision projects rapidly [19]. In this paper, the calibration is carried out using Halcon, and the camera calibration process is shown in Fig. 4.

(1) Select the appropriate camera and lens, and use the parameters of the camera and lens as the StartCamPar initial values. In this paper, the Daheng Mercury II MER2-2000-6GM industrial camera and Daheng HN-7531-20M-C1/1X lens, which are mounted on the end of the robot arm, are used.

(2) Select the calibration plate, generate the calibration plate description file through the operator gen_caltab, and select the path of the calibration plate description file at the initial calibration. In the calibration, an array of dot calibration plates, a circle with a diameter of 12.5mm, a process with a center distance of 25mm, and an alumina calibration plate with a thickness of 10mm are used.

(3) Selection of light source. Providing a light source can eliminate reflections and shadows. To ensure the stability and accuracy of the camera parameters effectively

$$\boldsymbol{R} = \begin{bmatrix} \cos\psi\cos\theta & \sin\psi\cos\theta & -\sin\theta \\ \cos\psi\sin\theta\sin\phi - \sin\psi\cos\phi & \sin\psi\sin\theta\sin\phi + \cos\psi\cos\phi & \cos\theta\sin\phi \\ \cos\psi\sin\theta\cos\phi + \sin\psi\sin\phi & \sin\psi\sin\theta\cos\phi - \cos\psi\sin\phi & \cos\theta\cos\phi \end{bmatrix} \tag{2}$$

improve the calibration accuracy, this paper adopts a strip light source, and the camera is on the same side of the calibration plate to light.

(4) Take calibration plate images. Fix the camera on the end of the robot and use the camera to take 20 pictures of the calibration plate. Each photo should be taken in different positions, angles, and attitudes. During the acquisition process, the calibration plate should be placed in the camera's field of view and occupy a large part of the image. At the same time, the lighting conditions should be ensured during the acquisition of ideas to ensure the accuracy of the calibration. The calibration plate calibrates the image, as shown in Figure 5.

(5) Extraction of calibration points. The centers of the separate array issues in the calibration plate are extracted and calibrated using the operator find_calib_object. In the get_calib_data_observ_contours and get_calib _data_observ_points, two operators are to get the calibration plate in the logo point contours and logo point center coordinates, extracted to the calibration plate above the target point.

(6) Camera calibration. The operator calibrate_cameras performs camera calibration, and the average projection error is also obtained.

(7) Aberration parameters. Use the operator get_calib_data to get the aberration parameters and finally save the parameters.

The camera's internal reference describes the geometrical properties of the camera and plays an essential role in hand-eye calibration. The transformation relationship between the robot end-effector and the camera can be calculated only by accurately obtaining the correct internal reference follow-up.

D. HAND-EYE CALIBRATION

Calibration of machine vision systems aims to convert between image coordinates and robot coordinate systems through camera and hand-eye calibration to realize collaborative work between machine vision and robots and improve the efficiency and accuracy of industrial automation. The camera calibration is a conversion between the pixel coordinate system and the calibration plate coordinate system. It can be obtained by acquiring the calibration plate image to its coordinates in three-dimensional space. Hand-eye calibration, on the other hand, converts the camera coordinate system and the tool coordinate system at the end of the robot to obtain the robot coordinate system corresponding to the image coordinates. In the hand-eye calibration system, the camera is fixed on the robot's end to establish the hand-eye calibration model. As shown in Figure 6.

According to the principle of coordinate system transformation, if the camera coordinate system is transformed concerning the robot end-effector coordinate system as Q_X:

$$Q_X = \begin{bmatrix} \mathbf{R}_X & \mathbf{t}_X \\ 0 & 1 \end{bmatrix} \tag{10}$$

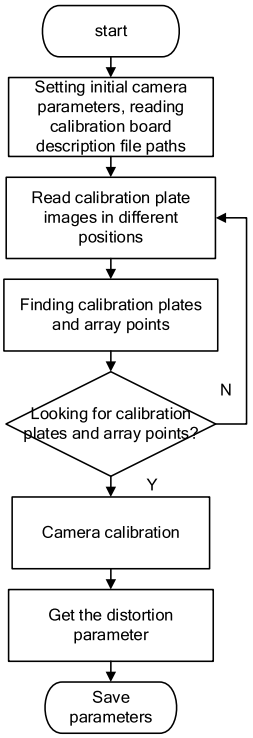

FIGURE 4. Flow chart of camera parameter calibration.

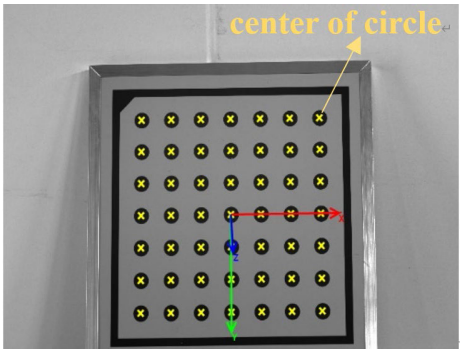

FIGURE 5. Calibration plate calibration image.

The transformation of the robot's end-effector coordinate system concerning the robot's base coordinate system is Q_r:

$$Q_r = \begin{bmatrix} \mathbf{R}_r & \mathbf{t}_r \\ 0 & 1 \end{bmatrix} \tag{11}$$

The transformation of the target object coordinate system concerning the camera coordinate system is Q_c:

$$Q_c = \begin{bmatrix} \mathbf{R}_c & \mathbf{t}_c \\ 0 & 1 \end{bmatrix} \tag{12}$$

The transformation of the target object coordinate system concerning the robot base coordinate system is Q_b:

$$Q_b = \begin{bmatrix} \mathbf{R}_b & \mathbf{t}_b \\ 0 & 1 \end{bmatrix} \tag{13}$$

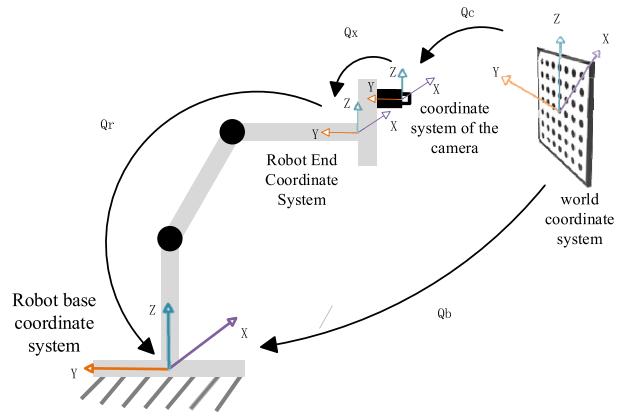

FIGURE 6. Hand-eye relationship model.

In the transformation matrix, R is a 3 × 3 unit orthogonal matrix representing the rotation relationship between coordinate systems; t is a vector representing the translation relationship between coordinate systems. According to the transformation relationship between the coordinate systems, the position matrix from the world coordinate strategy to the robot coordinate system can be obtained as follows:

$$Q_b = Q_r Q_x Q_c \tag{14}$$

By noting the current robot's bit position as 1, the bit position matrix from the world coordinate system to the robot coordinate system is:

$$Q_{b1} = Q_{r1} Q_x Q_{c1} \tag{15}$$

When the robot is in another bit-position recording that bit-position as 2, the bit-position matrix from the world coordinate system to the robot coordinate system is:

$$Q_{b2} = Q_{r2} Q_x Q_{c2} \tag{16}$$

Since the relative positions of the camera and the robot end-effector are kept constant, the transformation relation of the camera coordinate system concerning the robot end-effector coordinate system can be obtained as Q_c. It can be obtained from Eq. (15) and Eq. (16):

$$Q_{r1} Q_x Q_{c1} = Q_{r2} Q_x Q_{c2} \tag{17}$$

Multiplying both sides of Eq. (15) on the left and the right simultaneously yields:

$$Q_{r2}^{-1} Q_{r1} Q_x = Q_x Q_{c2} Q_{c1}^{-1} \tag{18}$$

Let $A = Q_{r1}^{-1} Q_{r1}$, $X = Q_x$, $B = Q_{c2} Q_{c1}^{-1}$, be obtained:

$$AX = XB \tag{19}$$

Equation (17) is the hand-eye calibration equation, which is decoupled by decomposing the fundamental equation of the hand-eye relationship into a rotation matrix and a translation matrix. Where then it can be obtained from equation (19):

$$\begin{bmatrix} R_A & t_A \\ 0 & 1 \end{bmatrix} \begin{bmatrix} R_X & t_X \\ 0 & 1 \end{bmatrix} = \begin{bmatrix} R_X & t_X \\ 0 & 1 \end{bmatrix} \begin{bmatrix} R_B & t_B \\ 0 & 1 \end{bmatrix} \tag{20}$$

Expressing the transformation matrix in Eq. (18) in terms of the corresponding rotation matrix and translation vectors leads to an expansion of the form [20]:

$$\begin{aligned} \boldsymbol{R}_A \boldsymbol{R}_X &= \boldsymbol{R}_X \boldsymbol{R}_B \\ \boldsymbol{R}_A t_X + t_A &= \boldsymbol{R}_X t_B + t_X \end{aligned} \tag{21}$$

In Eq. (19), R_B, T_B can be calculated from the motion parameters of the camera, R_A, t_A calculated from the joint angles read by the robot controller, and is the unknown quantity that needs to be solved for the hand-eye calibration, where R_X is the rotation matrix in the hand-eye relationship and is the translation vector in the hand-eye relationship. R_A, R_B, R_X are unit orthogonal matrices, indicating the rotation relationship between the coordinate systems; t_A, t_B, t_X are 3 × 1 vectors, meaning the translation relationship between the coordinate systems. The hand-eye calibration process is shown in Fig. 7.

1) Read camera parameters. The camera parameters derived from the calibration are read by the read_cam_par operator and brought into the hand-eye calibration program StartCamParam.
2) Acquisition of calibration plate images and robot position information. By acquiring 15 calibration plate images, the robot position information corresponding to each calibration plate image is recorded.
3) Create a hand-eye calibration model. Use the operator create_calib_data to create the hand-eye calibration model.
4) Set the calibration board description file. Set the corresponding file of the calibration plate in the calibration model using the set_calib_data_calib_object operator.
5) Image distortion correction. The operators change_radial_distortion_cam_par, and gen_radial_distortion_map are used to generate the internal reference without distortion, and map_image is used to correct the image with distortion and finally create the image without distortion for calibration.
6) Read the calibration plate image. Use find_calib_object to find the calibration plate in the picture, get_calib_data_observ_contours and get_calib_data_observ_points to get the points on the calibration plate, and finally display the coordinate information through the disp_3d_coord_system.
7) Hand-eye calibration calculation. Use calibrate_hand_eye to start using the calibration calculation, get_calib_data to get the parameters such as camera calibration error, camera internal parameters, and tool position, and finally save these parameters.

III. EXPERIMENTAL RESULTS AND ANALYSIS

The master gauge assists the user with camera focus adjustment, HUD eye box position alignment, and camera

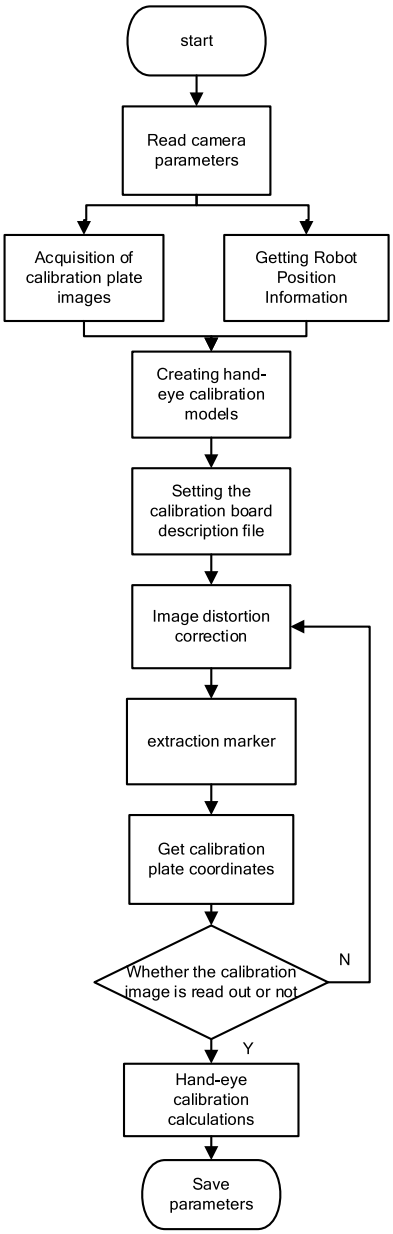

FIGURE 7. Flow chart of hand-eye calibration.

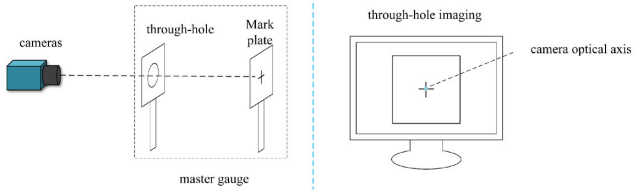

FIGURE 8. Diagram of calibration of master gauge.

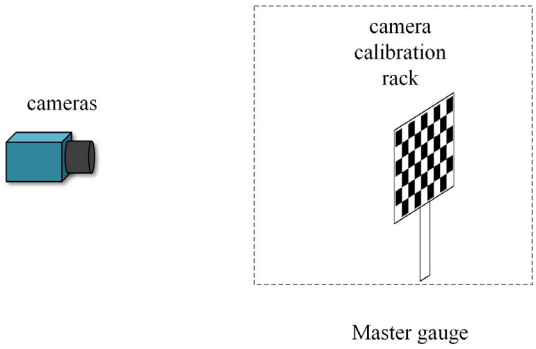

FIGURE 9. Master gauge camera calibration.

calibration functions primarily by providing essential visual markers such as the through-hole, cross Mark plate, and checkerboard pattern. Through the human eye to observe whether the cross position on the monitor is within the effective range of the through-hole, the error is generally considered to be 0 when the camera optical axis is aligned with the center of the cross. as shown in Figure 8.

During the camera calibration of the internal reference, the camera calibration sample frame, which is calibrated using a checkerboard grid pattern, is used to calculate the internal reference of the camera by directly photographing the rear of the camera on the master gauge with the camera. As shown in Figure 9

This scheme has some limitations, including the need to change and adjust the calibration frame frequently in different scenarios and applications. In addition, the calibration frame is less flexible and takes up more space, which makes it less suitable for mixed-line production of different vehicle models. Periodic calibration and maintenance are required to maintain the accuracy of the master gauge. However, the accuracy of calibration is influenced by the master gauge manufacturing process, design, and manufacturing accuracy standards. This means that if the master gauge manufacturing process or design standards do not provide a sufficiently high level of accuracy, then the accuracy of the calibration may be compromised. The use of calibration sample frames limits the flexibility of camera calibration, as in practice, situations may be encountered where the camera position needs to be adjusted quickly or calibrated in a dynamic environment. Such limitations may lead to reduced productivity and increased production costs.

This is in order to be used in subsequent automotive HUD calibrations to accurately solve for the camera coordinate system and the robot end tool coordinate system, as well as to provide accurate measurements for subsequent HUD shot maps for distortion correction. At the same time, camera calibration without a master gauge is usually more flexible and adaptable and can be used in a variety of environmental conditions. Calibration plate design and material selection can be optimized for specific environments. Camera calibration without a master gauge is more easily adapted to different operating environments than with a master gauge. The adaptability of the master gauge may be limited by environmental conditions and site constraints, especially in extreme conditions such as high temperatures or humid environments.

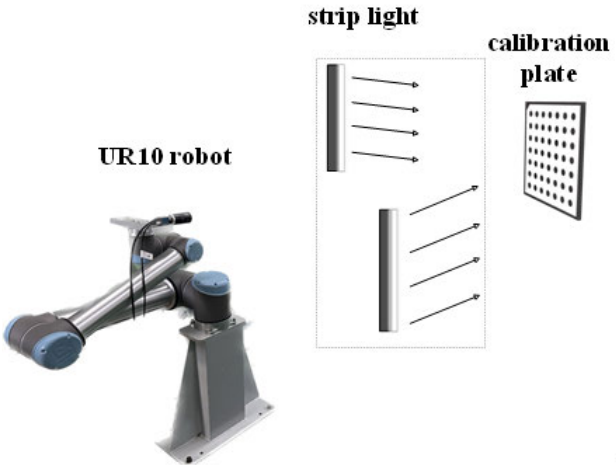

FIGURE 10. Hand-eye calibration experiment system.

TABLE 1. Experimental camera internal parameters.

camera parameters	Group 1	Group 2	Group 3
f(mm)	75.1426	75.3647	77.4088
$K_1(1/m^2)$	10.4099	19.0673	15.7437
$K_2(1/m^4)$	200393.8	-184542.6	-23431.7
$K_3(1/m^6)$	-5.24752e+09	5.92549e+08	-2.05232e+09
$P_1(1/m^2)$	-0.000966422	-0.0176387	-0.000499486
$P_2(1/m^2)$	0.0316183	0.0284144	0.0147587
S_x(um)	2.40296	2.39991	2.39796
S_y(um)	2.4	2.4	2.4
C_x(pixels)	2753.89	2936.25	2761.16
C_y(pixels)	2092.89	1870.67	1549.89
average error	0.156996	0.151696	0.13122

Mechanical components may be subject to expansion, contraction, or oxidation, causing the master gauge accuracy to suffer. Therefore, camera calibration without a master gauge helps to improve the robustness and performance stability of the automotive HUD inspection system.

In order to subsequently obtain more accurate HUD calibration results, the experiments in this paper use Universal-Robot-UR10 six degrees of freedom collaborative robot and Daheng Mercury II MER2-2000-6GM industrial camera, Daheng HN-7531-20M-C1/1X lens; the camera is fixed on the end of the robotic arm through the bracket, and it moves with the movement of the robotic arm, and the calibration plate uses the Array of dot calibration plate, the circle diameter is 12.5mm, the circle center distance is 25mm, and the thickness of the calibration plate is 10mm aluminum oxide calibration plate, and the strip light is used to lighten both sides. It is 12.5mm, the center distance of the circle is 25mm, and the thickness of the calibration plate is 10mm of aluminum oxide. The strip light is used to lighten both sides, as shown in Figure 10.

The distance between the camera and the calibration plate during the experiment was 2.3 m. Before performing hand-eye calibration, camera calibration is required to establish the interconversion relationship between the robot tool and camera coordinate systems. Three camera calibration images were collected, 20 in each group, and the in-camera parameters obtained through Halcon calibration are shown in Table 1.

In the above three groups of camera calibration experiments obtained by the camera calibration, the average error is about 0.15; calibration of high precision compared to the use of a master gauge for camera calibration is more flexible.

Compared with the camera calibration errors in literatures [21] and [22], we can observe that the average error in this paper is significantly reduced compared to the average errors in literature 24 and 25. The average error of the first group is reduced by 0.029432 and 0.008727 concerning literature 24 and literature 25, respectively. The average

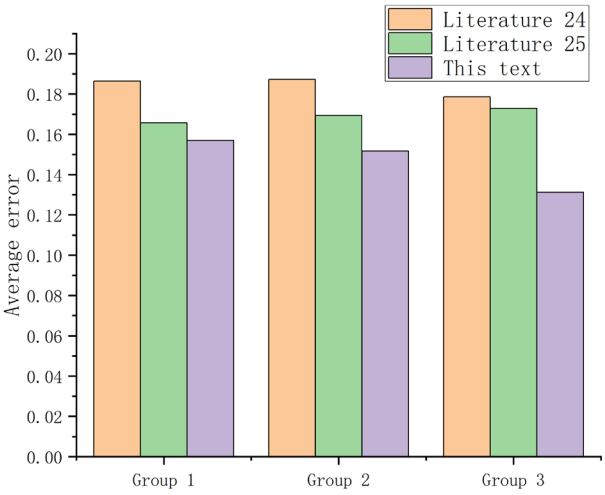

FIGURE 11. Comparison with literature camera calibration error results.

error of the second group is facilitated by 0.035593 and 0.017673 concerning literature 24 and literature 25, respectively. The average error of the third group is reduced by 0.047343 and 0.041737 concerning Literature 24 and Literature 25, respectively. Therefore, the camera calibration of the area_scan_polynomial model used in this paper has higher accuracy, as shown in Fig. 11.

To minimize the error of hand-eye calibration to get the hand-eye calibration results with higher calibration accuracy, this experiment selects the camera internal reference parameters obtained from the third group of camera calibration and brings the camera internal reference of the third group into the hand-eye calibration, and collects 12 groups of data in the experimental process, which is collected through the camera to collect 15 pictures of the calibration plate, and at the same time communicates with the robot to get the bit position corresponding to the 15 pictures using After writing a program in Python to convert the place into a format that Halcon can

TABLE 2. Experimental data for hand-eye calibration.

	Translational RMS	Translational Maximum	Rotational RMS	Rotational Maximum	Camera Calibration Error
1	0.508	0.850	0.023	0.044	0.0716
2	0.492	0.804	0.026	0.049	0.0719
3	0.476	1.002	0.023	0.037	0.0749
4	0.316	0.753	0.025	0.046	0.0725
5	0.386	1.043	0.028	0.062	0.0725
6	0.368	0.952	0.026	0.049	0.0736
7	0.426	0.67	0.04	0.07	0.0759
8	0.617	1.043	0.037	0.062	0.0743
9	0.694	1.068	0.038	0.061	0.0747
10	0.573	0.906	0.038	0.057	0.0740
11	0.57	1.173	0.038	0.068	0.0738
12	0.581	0.993	0.037	0.064	0.0732

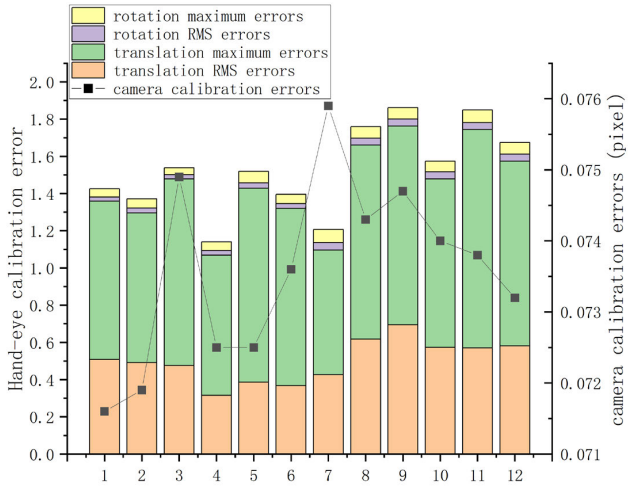

FIGURE 12. Histogram of hand-eye calibration error and a line graph of camera calibration error.

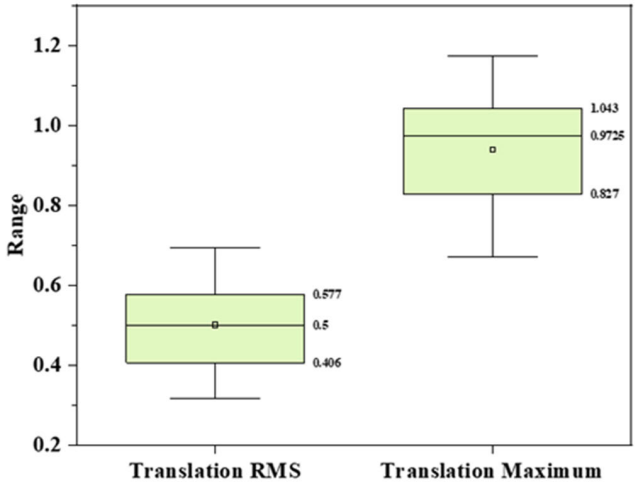

FIGURE 13. Hand-eye calibration Translation box line diagram.

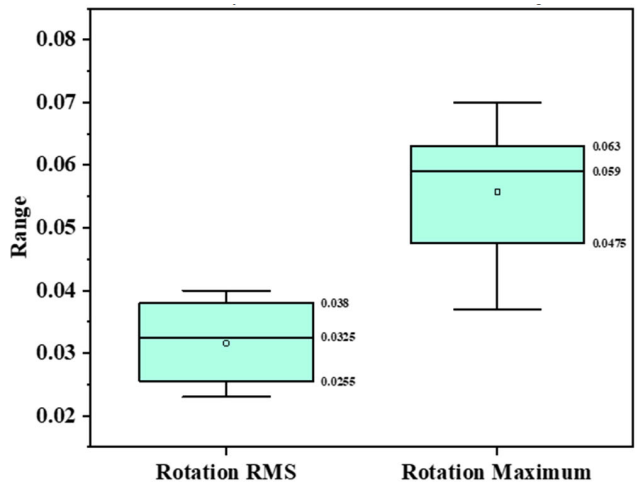

FIGURE 14. Hand-eye calibration of the Rotation box plot.

read, Halcon is used for hand-eye calibration. Finally, the relationship between the part of the robotic arm's end-effector and the camera's position is computed, that is, the coordinates and attitude of the end-effector of the robotic arm in the coordinate system of the camera. The hand-eye calibration position movement error, rotation angle error, and camera calibration error data in hand-eye calibration were calculated by collecting 12 sets of hand-eye calibration pictures and bit positions, as shown in Table 2.

The 12 data sets in Table 2 are made into a hand-eye calibration error map and a camera calibration error map, as shown in Figure 12. In Fig. 12, the maximum error value of the Translational part is about 1mm, the maximum error of the Rotational position is within 0.1°, and the camera calibration error is within 0.08 pixels, which makes the algorithm's conversion accuracy high enough to meet the requirements of collaborative robots in HUD. The main reasons that cause the calibration results still have errors are: (1) the long-distance hand-eye calibration is easily affected by the environmental lighting changes and other noises during the image acquisition process to produce calibration errors; (2) the accumulation of robotic arm errors affects the calibration results; (3) there are inherent errors in the camera; and (4) the calibration plate geometry, attitude, surface features, positional accuracy and other aspects of the error will have a calibration result deviation.

Also, based on the data in Table 2, boxplots are made for repeatability analysis, as shown in Fig. 13 and Fig. 14 for hand-eye calibrated boxplots. From Fig. 13, based on the boxplots, it is observed that the median of Translation RMS is 0.5, and the interquartile range (length of the box) is 0.171, which indicates that the data values of Translation RMS are relatively concentrated and stable. However, the Translation Maximum has a median of 0.972 and an interquartile range of 0.216. This indicates that the data values for Translation Maximum are relatively scattered and vary widely. Figure 14 Rotation boxplot analysis shows that Rotation RMS has a median of 0.0325 and an interquartile range of 0.0125. This indicates that the data values for Rotation RMS are relatively concentrated and stable. The median value of the Rotation

Maximum is 0.059, and the interquartile range is 0.016. This means that the data value of the Rotation Maximum is relatively concentrated and stable. In summary, the data in Translation is relatively more dispersed and has a more extensive range of variation but still maintains a certain degree of repeatability, and the data in Rotation is relatively more stable, with a smaller range of variation and better repeatability. Reasons affecting the repeatability: The larger RMS and Maximum values in Translation may be due to the longer distance between the calibration plate and the camera; the longer length may increase the measurement error and loss of precision, leading to the volatility of the results, as well as the ambient light interfering with the camera's perception and measurement during the experimental process, which affects the calibration results. In addition, factors such as camera lens distortion and robotic arm jitter may also affect the results of the translation part. In the rotation part, due to the calculation error of the rotation matrix, inaccuracy or instability of the rotation matrix, etc…Factors such as camera attitude error, insecure fixation of the calibration plate, etc., may also affect the rotation part's results.

IV. CONCLUDING REMARKS

Considering the general HUD system virtual image projection in 1.8-2.5 meters, in order to be able to use the collaborative robot in the HUD scene, this paper proposes the hand-eye calibration based on the monocular camera, placing the calibration plate at a distance of 2.3 meters away from the camera, in order to avoid the excessive influence of ambient lighting on the error, the paper adopts the customized alumina calibration plate, and through the appropriate angle of the light, the internal parameter of the camera is solved by adopting the area_scan_polynomial model for camera calibration. In order to avoid the influence of ambient light on the error, a customized aluminum oxide calibration plate is used in the paper, and by lighting at a suitable angle, the internal parameter of the camera is solved by using the area_scan_polynomial model for the camera calibration, and the solved internal parameter of the camera has an average error around 0.15, which makes the accuracy of the calibration higher and more flexible compared with that of using the master gauge for the camera calibration. The maximum error of the Translational part of the final hand-eye calibration solved is about 1mm, and the maximum error of the Rotational part of the error is within 0.1 degrees. The camera calibration error is within 0.08 pixels. Error is within 0.08 pixels, which has high accuracy; the data of Translation is relatively decentralized and has an extensive range of variation but still maintains a certain degree of repeatability, and the data of Rotation is relatively stable and has a small range of variation, which has good repeatability. As can be seen from the conclusion, a flexible calibration method for passenger car HUD inspection based on collaborative robots proposed in this paper is an excellent solution to the existing automotive industry vehicle final inspection of HUD, based on the Master Gauge calibration of the problems in the camera, through flexible calibration, the production line to expand the operating space, improve the accuracy of the inspection, and realize the multi-vehicle standard line pulsating production, but also applies to the new generation of virtual image projection distance It is also applicable to the new generation of augmented reality head-up display (AR-HUD) with a projection distance of about 7.5 meters, which further meets the requirements for the use of HUD in the final inspection scene of the whole vehicle.

REFERENCES

[1] Y.-F. Chiu and G.-D. J. Su, "Reduce, volume of head-up display by image stitching," *Proc. SPIE*, vol. 9947, pp. 123–133, Sep. 2016.
[2] C.-T. Mu, W.-T. Lin, and C.-H. Chen, "Zoomable head-up display with the integration of holographic and geometrical imaging," *Opt. Exp.*, vol. 28, no. 24, pp. 35716–35723, 2020.
[3] Q. Jiang and Z. Guo, "AR-HUD optical system design and its multiple configurations analysis," *Photonics*, vol. 10, no. 9, p. 954, Aug. 2023.
[4] L. Yu, "Analysis of present status of imaging parameter measurement technology in head-up display system," *Laser J.*, vol. 41, no. 2, pp. 5–10, 2020.
[5] Z. Xiaofeng, L. Changqing, C. Wei, and W. Yinpeng, "Research on brightness perception model based on night vision vehicle head up display," *Laser Optoelectron. Prog.*, vol. 54, no. 12, 2017, Art. no. 121501.
[6] L. Jun and T. Miao, "The optical system design of the HUD parallax measurement," *J. Xi'an Technol. Univ.*, vol. 28, no. 6, pp. 521–525, 2008.
[7] R. Y. Tsai and R. K. Lenz, "A new technique for fully autonomous and efficient 3D robotics hand/eye calibration," *IEEE Trans. Robot. Autom.*, vol. 5, no. 3, pp. 345–358, Jun. 1989.
[8] J. C. K. Chou and M. Kamel, "Finding the position and orientation of a sensor on a robot manipulator using quaternions," *Int. J. Robot. Res.*, vol. 10, no. 3, pp. 240–254, Jun. 1991.
[9] K. Daniilidis, "Hand-eye calibration using dual quaternions," *Int. J. Robot. Res.*, vol. 18, no. 3, pp. 286–298, Mar. 1999.
[10] A. Malti and J. P. Barreto, "Robust hand-eye calibration for computer aided medical endoscopy," in *Proc. IEEE Int. Conf. Robot. Autom.*, May 2010, pp. 5543–5549.
[11] N. Andreff, R. Horaud, and B. Espiau, "On-line hand-eye calibration," in *Proc. 2nd Int. Conf. 3-D Digit. Imag. Model.*, 1999, pp. 430–436.
[12] L. Aiguo, W. Lin, and W. Defeng, "Simultaneous robot-world and hand-eye calibration using dual-quaternions and Kronecker product," *Int. J. Phys. Sci.*, vol. 5, no. 10, pp. 1530–1536, 2010.
[13] Z. Zhao, "Hand-eye calibration using convex optimization," in *Proc. IEEE Int. Conf. Robot. Autom.*, May 2011, pp. 2947–2952.
[14] W. Long, J. Jiao, X. Liang, T. Wu, M. Xu, and S. Cai, "Pinhole-imaging-based learning butterfly optimization algorithm for global optimization and feature selection," *Appl. Soft Comput.*, vol. 103, May 2021, Art. no. 107146.
[15] O. D. Faugeras, "The calibration problem for stereo," in *Proc. IEEE Conf. Comput. Vis. Pattern Recognit.*, Jun. 1986, pp. 15–20.
[16] Y.-J. Zhang, *Camera Calibration, 3-D Computer Vision: Principles, Algorithms and Applications*. Berlin, Germany: Springer, 2023, pp. 37–65.
[17] Q. Zhenqi, "Study of single camera calibration based on HALCON software," *J. Shijiazhuang Tiedao Univ.*, vol. 31, no. 3, pp. 75–80, 2018.
[18] Y. Houyi, "Accuracy analysis and inversion method of robot hand-eye calibration based on Halcon," *Inf. Technol. Netw. Secur.*, vol. 37, no. 1, pp. 97–100, 2018.
[19] L. Ke, "Realization of halcon image segmentation algorithm in machine vision for complex scenarios," in *Proc. 3rd Int. Conf. Artif. Intell. Smart Energy (ICAIS)*, Feb. 2023, pp. 1112–1116.
[20] J. Jiang, X. Luo, S. Xu, Q. Luo, and M. Li, "Hand-eye calibration of EOD robot by solving the AXB = YCZD problem," *IEEE Access*, vol. 10, pp. 3415–3429, 2022.
[21] C. Tian, L. Chen, G. Ma, M. S. Hou, and T. Liu, "Research on hand-eye calibration method of industrial robot based on Halcon," *Manuf. Autom.*, vol. 40, no. 3, pp. 16–18&46, 2018.
[22] T. Hao, "Calibration method of machine vision system based on ALCON," *J. Liaoning Univ. Technol.*, vol. 40, no. 4, pp. 211–215&235, 2020.

DING ZHIGANG received the master's degree in bioengineering from Jilin University, in 2007. He has been a Senior Engineer with the Fujian University of Technology, since 2008. He is currently the Head of the Vehicle Engineering Laboratory. He has participated in more than ten national 863 programs and provincial and municipal scientific research projects. He is mainly engaged in the research and development of new energy vehicle power system assembly, product visual inspection, and intelligent equipment.

YANLU LV was born in Xiamen, Fujian, in1997. He received the bachelor's degree in mechanical manufacturing and automation from the School of Physics and Electromechanics, Longyan University. He is currently pursuing the master's degree in mechanical engineering with the School of Mechanical and Automotive Engineering, Fujian University of Technology. His research interests include machine vision and image processing.

LINGHUA KONG received the bachelor's degree in physics from Nankai University, in 1983, the master's degree in physics from the Institute of High Energy Physics, Chinese Academy of Sciences, in 1988, and the Ph.D. degree in mechanical engineering from the Department of Mechanical Engineering, McGill University, Canada, in 2004. He received a Postdoctoral Fellowship with the Georgia Institute of Technology, in 2005. He is currently a Professor with the School of Mechanical and Automotive Engineering, Fujian University of Technology. He designed and developed a variety of new products and equipment, and obtained 15 patents: published 20 influential articles included in SCI/EI as the first author. His main research interests include multispectral and plasma fields.

ZHIMING DONG is currently pursuing the master's degree in computer technology with the School of Transportation, Fujian University of Technology. He mainly studies directional machine vision.

JISHI ZHENG received the Ph.D. degree from Central South University, China, in 2015. From January to July 2019, he was a Visiting Scholar with the Robotics Laboratory, Computer and Electronic Engineering Department, University of Essex, U.K. He is with the Fujian University of Technology, where he is currently the Head of the Internet of Things major, the Director of Teaching and Research with the Department of Traffic Information and Control, and the Executive Director of the Fujian Society of Aeronautics. He has presided over and participated in more than ten provincial and municipal scientific research projects. His main research interests include application of artificial intelligence in the industry and research of UAV flight control algorithm.

JIADI ZHANG is currently the Legal Representative of Xiamen Richen Technology Company Ltd., Chengdu Branch, which is a high-tech enterprise specializing in factory automation and factory digitalization, online detection, and robot-assisted production, with independent intellectual property rights and independent research and development capabilities.

JIAXIN LIU is currently pursuing the master's degree in mechanics with the Fujian University of Technology. His main research interests include machine vision and deep learning.